Available online at www.sciencedirect.com

ScienceDirect

www.elsevier.com/locate/jes

JES JOURNAL OF ENVIRONMENTAL SCIENCES www.jesc.ac.cn

Effect of temperature tuning on the aerosol acoustic aggregation process

Zhenghui Qiao[1], *Wei Dong*[1,2,*], *Yaji Huang*[1], *Vincenzo Naso*[2]

1. *Key Laboratory of Energy Thermal Conversion and Control of Ministry of Education, School of Energy & Environment, Southeast University, Nanjing 210096, China. E-mail: seuqzh@seu.edu.cn*

2. *Department of Mechanical and Aerospace Engineering, SAPIENZA University of Rome, Via Eudossiana, 18-00184 Rome, Italy*

ARTICLE INFO

Article history:
Received 26 April 2017
Revised 26 August 2017
Accepted 28 August 2017
Available online 1 September 2017

Keywords:
Diesel exhaust
Acoustic field
Aggregation
Acoustic standing wave
Temperature
Nanoparticles

ABSTRACT

Diesel exhaust aerosols (DEAs) can absorb and accumulate toxic metal particulates and bacteria suspended in the atmospheric environment, which impact human health and the environment. The use of acoustic standing waves (ASWs) to aggregate DEA is currently considered to be an efficient particle removal method; however, study of the effect of different temperatures on the acoustic aggregation process is scarce. To explore the method and technology to regulate and optimize the aerosol aggregation process through temperature tuning, an acoustic apparatus integrated with a temperature regulation function was constructed. Using this apparatus, the effect of different characteristic temperatures (CTs) on the aerosol aggregation process was investigated experimentally in the ASW environment. Under constant conditions of acoustic frequency 1.286 kHz, voltage amplitude 17 V and input electric power 16.7 W, the study concentrated on temperature effects on the aggregation process in the CT range of 58–72°C. The DEA opacity was used. The results demonstrate that the aggregation process is quite sensitive to the CT, and that the optimal DEA aggregation can be achieved at 66°C. The aggregated particles of 68.17 μm are composed of small nanoparticles of 13.34–62.15 nm. At CTs higher and lower than 66°C, the apparatus in non-resonance mode reduces the DEA aggregation level. For other instruments, the method for obtaining the optimum temperature for acoustic agglomeration is universal. This preliminary demonstration shows that the use of acoustic technology to regulate the aerosol aggregation process through tuning the operating temperature is feasible and convenient.

Introduction

The diesel engine, as a type of combustion engine, is widely used in transportation areas, and has become a troublesome soot emitter for the atmospheric environment. Numerous diesel exhaust aerosols (DEAs), commonly with submicron size, (Guan et al., 2015; Burtscher, 2005; Kittelson, 1998; Harris and Maricq, 2001; Wang et al., 2012) are exhausted into the environment, which exacerbates the atmospheric particle pollution, such as the particulate matter of diameter less than 2.5 μm ($PM_{2.5}$) level. Acoustic removal (Chen et al., 2009, 2015; Gallego-Juarez et al., 1999; González et al., 2003; Guo et al., 2012; Liu et al., 2009, 2011; Noorpoor et al., 2012; Sheng and Shen, 2007; Sun et al., 2013; Yuen et al., 2014) enhances the growth process from small to large aerosol particles by means of acoustic standing waves (ASW) impacts. The process through which the ASW interacts with DEA is generally referred to as acoustic aggregation. Chen et al. (2009) found that the particle size

* *Corresponding author*. E-mail: dongwei59@seu.edu.cn (Wei Dong).

http://dx.doi.org/10.1016/j.jes.2017.08.021

distribution of the ultrafine particles in diesel engine exhaust can be markedly changed by ASW at room temperature. Noorpoor et al. (2012) asserted that the ASW field can coagulate nano-particles in diesel exhaust in order to become larger size under any temperature condition. In addition, many researchers, for example, Chen et al. (2015), Sun et al. (2013), Guo et al. (2012), Liu et al. (2009, 2011) and Gallego-Juarez et al. (1999), have verified that coal-fired flue ash can be significantly removed by an enhanced process of acoustic aggregation. Chen et al. (2015) proposed that the coupling of the acoustic and electric environment can efficiently remove fine particles from coal combustion. Yuen et al. (2014) proposed that nonlinear acoustics can act as an energy-efficient technique to enhance the aerosol removal process. Sun et al. (2013) proposed that the coupling effect between a gas jet and acoustic wave can also efficiently remove coal-fired particles. Qiao et al. (2015) proposed that the structural parameters of the acoustic resonant field can enhance the spatial distribution of aerosols and result in the X-pattern distribution phenomenon. In the above studies, temperature is commonly considered as an important factor (Noorpoor et al., 2012; Sheng and Shen, 2007; Liu et al., 2009; González et al., 2003) impacting the effect of aerosol removal in an ASW field, yet relevant experimental studies investigated the removal process under a constant temperature condition. Study on the effect of different temperatures on the removal process is scarce. Considering the importance of the temperature factor on the acoustic aggregation process, it is necessary to study the potential effects of temperature on the aerosol aggregation process in an acoustic field, which is the objective of this paper.

In recent studies on aerosol removal by ASW (Chen et al., 2009, 2015; Gallego-Juarez et al., 1999; Guo et al., 2012; Liu et al., 2009, 2011; Noorpoor et al., 2012; Qiao et al., 2014, 2015; Sheng and Shen, 2007; Sun et al., 2013; Yao et al., 2010; Yuen et al., 2014), the particle size distribution is generally considered an indispensable factor to reflect the change of aerosol behavior characteristics. One important reason is that smaller aerosols (such as those with particle size less than 2.5 μm) cannot be completely removed by the traditional particle removal apparatus (Yao et al., 2010). The second is that the particle size distribution of aerosols can clearly change under the influence of ASW. In addition, aerosol opacity is an important index to determine the concentration of aerosols (Kumar et al., 2005; Zajac, 2008; Czechlowski et al., 2015). The mechanism is based on the light penetrability of smoke with different aerosol concentrations. A higher opacity corresponds to a higher concentration of aerosol. Notably, the aerosol opacity is currently considered as a control index to assess the emission performance of diesel exhaust (Sae, 1996). Accordingly, in this paper we will utilize the opacity to characterize the aerosol concentration variation with different characteristic temperatures (CTs) given by a temperature tuning platform.

In our previous study, we invented a new apparatus for generating an ASW field (Qiao et al., 2014, 2015). The performance in aerosol removal has been tested for tobacco smoke (Qiao et al., 2014). Based on the apparatus, a new apparatus for generating an ASW field with optimal temperature control was constructed to explore the effect of temperature on the acoustic aggregation process for DEA. The DEA aggregation process was investigated at six different CTs in the range of 58–72°C. The corresponding DEA opacity variation was used to evaluate the effect on the DEA aggregation process. Especially, we emphasize the interesting potential of the enhancement of the acoustic aggregation level by means of temperature tuning.

1. Experiment and method

1.1. Experimental apparatus

The laboratory experimental unit was constructed, and the main configuration of the acoustic apparatus with the temperature tuning platform is shown in Fig. 1. The composite image composed of images A, B and C simply represents the apparatus configuration for generating an ASW field with optimal temperature control. The ASW field in the cylindrical aerosol chamber (CAC) is regulated and controlled with a pair of opposing Helmholtz resonant sources (HRS) composed of a Helmholtz resonator (HR) and speaker (Qiao et al., 2014, 2015). The HRS based on acoustic streaming causes a large acoustic pressure. The dashed arrow demonstrates the supply process for the sinusoidal alternating-current (AC) voltage signal from the signal generator and amplifier to the speaker. The temperature tuning platform composed of heating tape, temperature controller and thermocouple has the function of conveniently regulating and controlling the heating temperature. The heating tape is wrapped on the wall of the CAC to form a steady operating temperature environment in it. The heating temperature of the heating tape is regulated by the temperature controller by manipulating the warming-up time. The thermocouple for measuring CT is mounted on the interface between the heating tape and the outside surface of CAC at position D (see image B). The dash dot line demonstrates the process of temperature regulation and control. The double dash line represents the signal wire of the thermocouple. The opacity measurement system consists of a smoke opacity meter (SV-5Y, Tianjin Shi Shengwei Development of Science Company Limited, China) and exhaust gas analyzer (SV-5Q, Tianjin Shi Shengwei Development of Science Company Limited, China). The sampling probe of the smoke opacity meter is inserted into the cushion chamber to extract DEA. The opacity data measured by the smoke opacity meter is analyzed and recorded by the exhaust gas analyzer. The measured precision of the opacity is ±0.2%. The solid line arrow demonstrates the flow direction of diesel exhaust in each component. At the smoke entrance of position F (see image C), the smoke exhausted from diesel is drawn into the CAC by an exhaust separator. After the action of ASW field at a specific temperature condition in CAC, the diesel exhaust is discharged into the cushion chamber. The cushion chamber is used for the DEA sampling of the opacity measurement system. The smoke output of the CAC is arranged at position E (see image A), as the sampling point for the opacity measurement. This point represents the average position between the adjacent nodal point and anti-nodal point of ASW.

For the experiment parameters of the diesel engine, the torsion is 19.9 N·m, and the load is 17%; the engine speed is 1204 r/min; the power is 2.51 kW; the fuel consumption is 403.5 g/kWh. For the experimental parameters of the acoustic sources, the voltage amplitude and the total electrical power input of the signal supplied from the amplifier to the speakers is 17 V and 16.7 W, respectively. During the acoustic aggregation experiment at all CTs, the acoustic frequency is constant, always

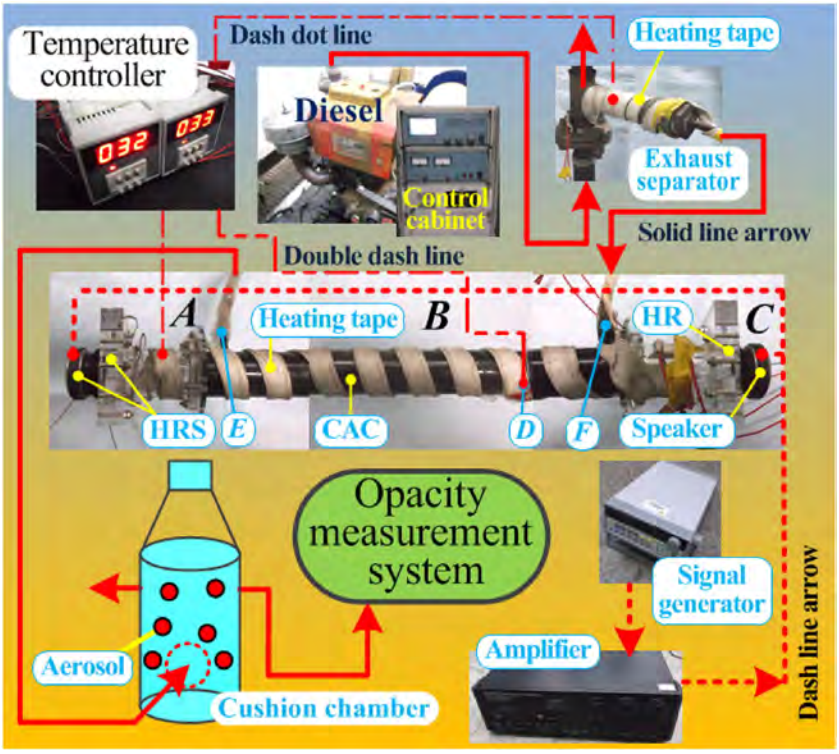

Fig. 1 – Schematic diagram of experimental apparatus. The main component images A, B and C of acoustic apparatus composed by opposing HRS (in A and C) and CAC (in B); HRS: Helmholtz resonant source; CAC: cylindrical aerosol chamber; position D of the thermocouple; the positions of entrance (F) and output (E) of CAC; HR: Helmholtz resonator.

equaling the driving frequency 1.286 kHz of the speakers; the voltage amplitude, the input electric power and the geometric parameters of the apparatus are also kept constant. For the temperature parameters, the steady temperatures measured inside CAC at each CT are respectively 47.2 ± 0.4°C at 58°C, 50.3 ± 0.1°C at 64°C, 52.2 ± 0.3°C at 66°C, 53.5 ± 0.5°C at 68°C, 55.5 ± 0.5°C at 70°C and 57.5 ± 0.5°C at 72°C. Note that the directly measured CT indicates the specific wall temperature of the CAC. Due to the thermal resistance between the wall and host fluid medium, the CT is different from the steady temperature of the diesel exhaust inside the CAC. The CT is defined to distinguish the two temperatures.

1.2. Method

1.2.1. Mechanism of aerosol aggregation

The DEA aggregation process is strongly affected by complex experimental conditions such as pressure, temperature, humidity and so on. According to the theory of acoustic aggregation (Noorpoor et al., 2012; Sheng and Shen, 2007), the collision and growth process of small aerosols in diesel exhaust can be affected by regulating the temperature of the diesel exhaust. However, the effect of temperature on acoustic aggregation is mainly attributed to Brownian diffusion (Noorpoor et al., 2012), yet is rarely attributed to the acoustic resonance (Johansson et al., 2013). The comprehensive mechanism of acoustic aggregation for inhalable particles such as DEA needs further exploration (Guo et al., 2012). In particular, the practical aerosol trapping and agglomeration at the nodal points of ASW is not necessarily contained in this regime (Hawkes and Radel, 2013). On the other hand, the acoustic radiation force has recently been indicated as an efficient mechanism for particle aggregation in the fluid of an ASW environment (Ahn et al., 2014; Karpul et al., 2010; Laurell et al., 2007; Kozuka et al., 2007; Yuen et al., 2014; Hammarström et al., 2012; Qiao et al., 2014; Cheng et al., 2016). On the basis of this mechanism, the proper temperature requirement can regulate the specific trapping efficiency for small particles in an ASW fluid (Johansson et al., 2013). Considering that the particle size of DEA is much smaller than the ASW wavelength of generated in the apparatus, 279 mm, the acoustic radiation force introduced by Bruus (2012) is suitable for the working principle of our apparatus.

According to the Gor'Kov (1962) suggestion that the aerosol geometry should be a compressible sphere, Bruus (2012) expressed the acoustic radiation force F^{rad} (N) of the ASW on a single, small sphere as,

$$F_z^{rad} = -\partial_z U^{rad}, \tag{1}$$

$$U^{rad} = \left[\frac{f_1}{3}\cos^2(kz) - \frac{f_2}{2}\sin^2(kz)\right] \times \pi a^3 \kappa_0 p_a^2, \tag{2}$$

$$f_1(\tilde{\kappa}) = 1 - \tilde{\kappa}, \quad \text{where } \tilde{\kappa} = \frac{\kappa_p}{\kappa_0}, \tag{3}$$

$$f_2(\tilde{\rho}) = \frac{2(\tilde{\rho}-1)}{2\tilde{\rho}+1}, \quad \text{where } \tilde{\rho} = \frac{\rho_p}{\rho_0}. \tag{4}$$

Here, k (m^{-1}) is the wavenumber of the acoustic wave; z (m) is the axial coordinate of CAC; a (m) is the radius of the spherical aerosol; p_a (Pa) is the amplitude of the acoustic pressure; κ_0

(Pa^{-1}) and κ_p (Pa^{-1}) are the compressibility of the host fluid medium and the aerosol, respectively; ρ_0 (kg/m^3) and ρ_p (kg/m^3) are the density of the host fluid medium and the aerosol, respectively.

A number of reports (Ahn et al., 2014; Laurell et al., 2007; Hammarström et al., 2012; Karpul et al., 2010; Kozuka et al., 2007; Weiser et al., 1984; Yuen et al., 2014; Foresti et al., 2013; Johansson et al., 2013; Bruus, 2012; Gor'Kov, 1962) have indicated that DEA exposed to the ASW environment with different temperature parameters is subjected to the action of the acoustic radiation force. The DEA is trapped at the nodal points of the ASW due to acoustic radiation force, and particles agglomerate with each other, which contributes to the aerosol aggregation process (Ahn et al., 2014; Laurell et al., 2007; Weiser et al., 1984; Hammarström et al., 2012; Kozuka et al., 2007; Yuen et al., 2014; Gallego-Juarez et al., 1999; Johansson et al., 2013).

Because the experimental apparatus can be considered an acoustic resonator, the acoustic pressure in the CAC depends on how close the drive frequency is to its resonant frequency. The resonant frequency f_r (kHz) of CAC is a function of the speed of sound in a fluid medium, and the sound speed depends on the steady temperature T (°C) measured in the CAC. The relation between the resonant frequency and the temperature is expressed as (Beranek, 1954).

$$f_r = n(331.4 + 0.607\,T)/(2\,L). \quad (5)$$

Here, $n = 7$ and $L = 978$ mm are respectively the harmonic order and the length of the CAC. Using Eq. (5), the variation of the resonant frequency with CT can be calculated. The experimental values of the resonant frequency can be found by the measured frequency response curves of acoustic pressure at different CTs. The frequency value corresponding to the peak in the measured curve is the experimental resonant frequency at each CT. It can be seen from Fig. 2 that the calculated and experimental trend lines are approximately parallel. For each CT, the calculated value of the resonant frequency is close to the experimental value.

For measurement of the frequency response curve at each CT, the change range of the drive frequency is from 1.21 to 1.33 kHz. In the constant voltage amplitude and input electric power of speakers, for each drive frequency and each CT, the amplitude p_a of acoustic pressure can be measured by using acoustic pressure meters (Qiao et al., 2014) and considered as the maximum acoustic pressure P in CAC. For different drive frequencies, many different maximum acoustic pressures P can be acquired at different CTs, in which the maximum value of all P is defined as P_{max}. Each P can be normalized by the ratio P/P_{max}.

The influence of the CT on the acoustic pressure amplitude p_a is shown in Fig. 3. As an example, the curves for the acoustic pressure ratios in Fig. 3a represent the different frequency responses of acoustic pressure at different CTs. For each response curve, there always exists one resonant frequency corresponding to a peak value. When the drive frequency of the input signal equals the resonant frequency, resonance occurs. When the drive frequency is lower or higher than this frequency, sub- or super-resonances occur, respectively. Due to the different resonant frequencies at different CTs, under the constant drive frequency of 1.286 kHz the maximum acoustic pressures are different, as shown in Fig. 3b. At the CT of 66°C, the acoustic pressure with CTs achieves the peak value.

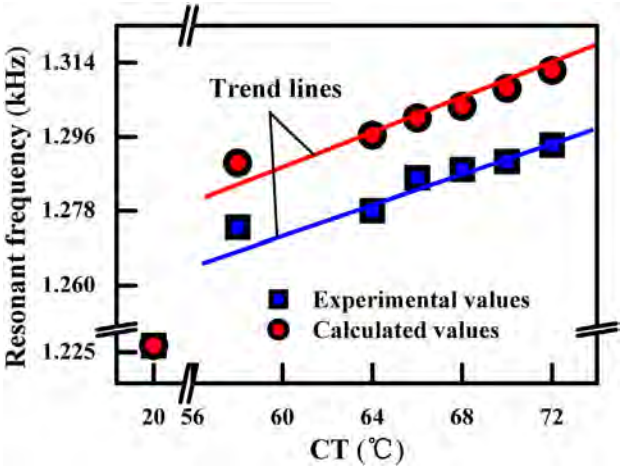

Fig. 2 – Resonant frequency variation with CT (characteristic temperature).

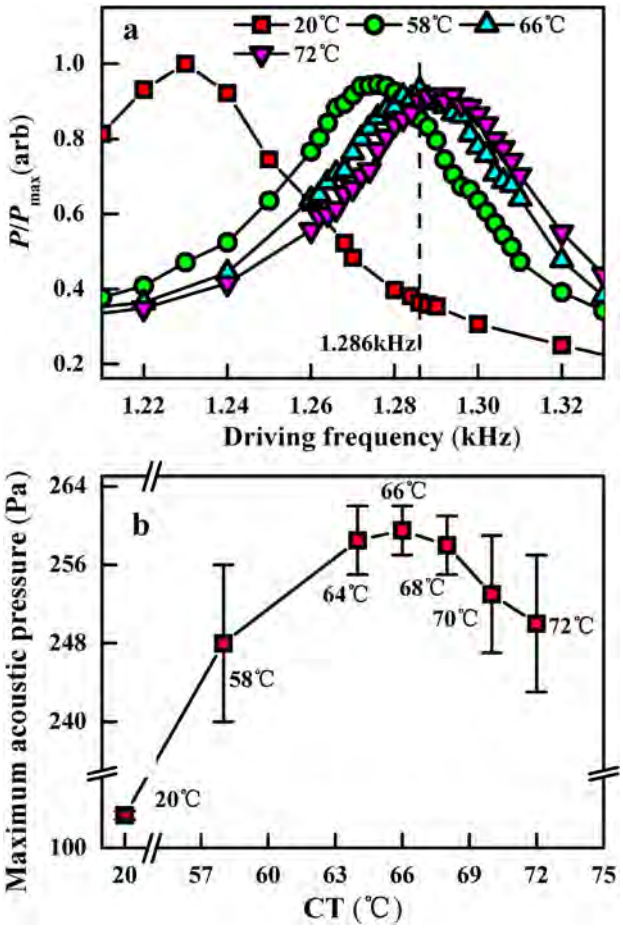

Fig. 3 – Temperature dependence of acoustic pressure. (a) Resonant response; (b) acoustic pressure change. P: the maximum acoustic pressure at one drive frequency and one CT; P_{max}: the maximum value of P; P/P_{max}: the acoustic pressure ratio.

Accordingly, the aerosol aggregation process under the action of ASW can be optimized by the temperature regulation and control. When the CT changes, the intensity of the aerosol collision and growth process will change. The number concentration of aerosols is changed with the change in intensity.

1.2.2. Opacity data processing

Particles can scatter light when they alter the direction of radiation beams without absorbing radiation, which is the principal mechanism for limiting the visibility of the atmosphere. The scattering of light by air molecules is inefficient because their size is orders of magnitude smaller than the wavelengths of visible radiation (0.4–0.7 μm). Due to the large size of aerosols, the visibility is reduced significantly. The value of the smoke opacity meter varies with the DEA concentration. The measured opacity variation represents the DEA concentration variation at different CTs. Through continuous measurement of opacity, a series of discrete data can be taken at each CT. The aerosol aggregation processes at different CTs are indirectly reflected in the tested opacity data time series.

For the discrete time-domain information $x(t)$, the frequency-domain information based on discrete Fourier transformation can be analyzed as in Eqs. (6a) and (6b),

$$S_{xx}(w) = \frac{1}{N}\sum_{y=0}^{N-1} Y_{xx}(y)\ \exp(-i2\pi wy/N), \tag{6a}$$

$$Y_{xx}(y) = \frac{1}{N}\sum_{j=0}^{N-y} x(j)x(j+y) \quad (y = 0, 1, 2, \cdots, m). \tag{6b}$$

Here, $S_{xx}(w)$ is the power spectrum density for the opacity data time series; $x(j)$, equivalent to $x(j\Delta t) = x(t)$, is the discrete time series data for the tested opacity; $Y_{xx}(y)$ is equivalent to $Y_{xx}(y\Delta t) = Y_{xx}(\tau)$; τ is the moving value of the time coordinate; Δt is the time interval for collecting the sample; $N = T_2/\Delta t$ is the total amount of sample collected, T_2 is the total time for sample collection. Due to the practical complexity of Eq. (6a), the $S_{xx}(w)$ can be solved by the fast Fourier transform algorithm. The power spectrum density in the frequency-domain information reveals the potential periodic characteristics of irregular opacity time-domain information acquired from the practical complex process of aerosol aggregation.

For the discrete time-domain data $x(t)$, the probability distribution function is expressed as Eq. (7),

$$P(X \le x, T_3) = \frac{N_1}{N}. \tag{7}$$

Here, $X = \{x(t)\}$ is the collective sample function. At the moment of T_3, the sample frequency for the sample function with value no greater than the designated value x is N_1, which is the accumulation frequency for the sample variable. Eq. (7) is the distribution function of the discrete opacity variable X, and demonstrates the normalization method for the sample frequency N_1. Depending on the variation of the distribution function with the designated opacity value x, the discrete opacity data at different CTs is compared by calculating the normalized frequency. Such comparison reveals the hidden regulation in the numerous opacity time-series data.

2. Analysis and discussion of tested results

2.1. Difference in the aerosol opacity between two CTs

Fig. 4 shows the characteristics of the DEA opacity responses at 66 and 70°C during data collection duration more than 9 min. Just as shown in Fig. 4a and b, the opacity response has two characteristic values, 67.5% (average) and 23.8% (average), at 66 and 70°C. These two characteristic values approximately constitute the series data for the opacity in the time domain. The time-domain information is obviously different at 66 and 70°C. The opacity at 66°C is generally greater than that at 70°C. The smaller the average time-interval is for opacity greater than 60% during the data collection, the greater the time-interval density is for the observation of opacity greater than 60%. It is obvious that the time-interval density at 66°C is much larger than that at 70°C. However, the instantaneous variation of the time-interval at each CT appears complex.

For exploring the regularity in the variation of the complex opacity data, the time period of the opacity data is shown in Fig. 4c to g. Considering the frequency-domain information to be completely equivalent to time-domain information, based on Eq. (6a) and (6b), the time period characteristic of the opacity in the time domain at different temperatures is quantified accurately by a fast Fourier transform. Fig. 4g shows that the power spectrum is different at 66 and 70°C. The intensity of the power spectrum at 66°C is seemingly greater than that at 70°C. The quantitative difference between the two spectra indicates that the time period is extraordinarily different at 66 and 70°C.

On the basis of the time series data for the measured opacity at 66 and 70°C, the difference obtained from the two-aspect analysis of the time-domain and the frequency-domain verifies experimentally the different particle variation characteristics in the aggregation processes at different temperatures. Due to the different time-interval densities and the different time period, the actual particle concentration variations at 66 and 70°C are different in the complex experimental acoustics-temperature-particle physics system. According to the aerosol aggregation mechanism stated in Section 1.2.1, this difference reveals the different DEA growth processes for aggregation at 66 and 70°C. Considering the attenuation of light propagation by high concentration DEA, the high time-interval density for the opacity data at 66°C indicates the growth process of DEA to be violent. The opacity characteristic value of 67.5% corresponds to a higher DEA concentration compared with that corresponding to the characteristic value of 23.8%. Combined with the extraordinarily different time period, the measured time series opacity data indicates the complex temperature effect on the aggregation process. Note that the quantitative high intensity of the power spectrum at 66°C corresponds to this violent aggregation process, in spite of the existence of several low power values at frequencies close to 7.5 min^{-1} shown in Fig. 4g. The difference in intensity for the power spectra analyzed by Fourier transform approximately corresponds to the quantitative DEA aggregation difference at the two CTs.

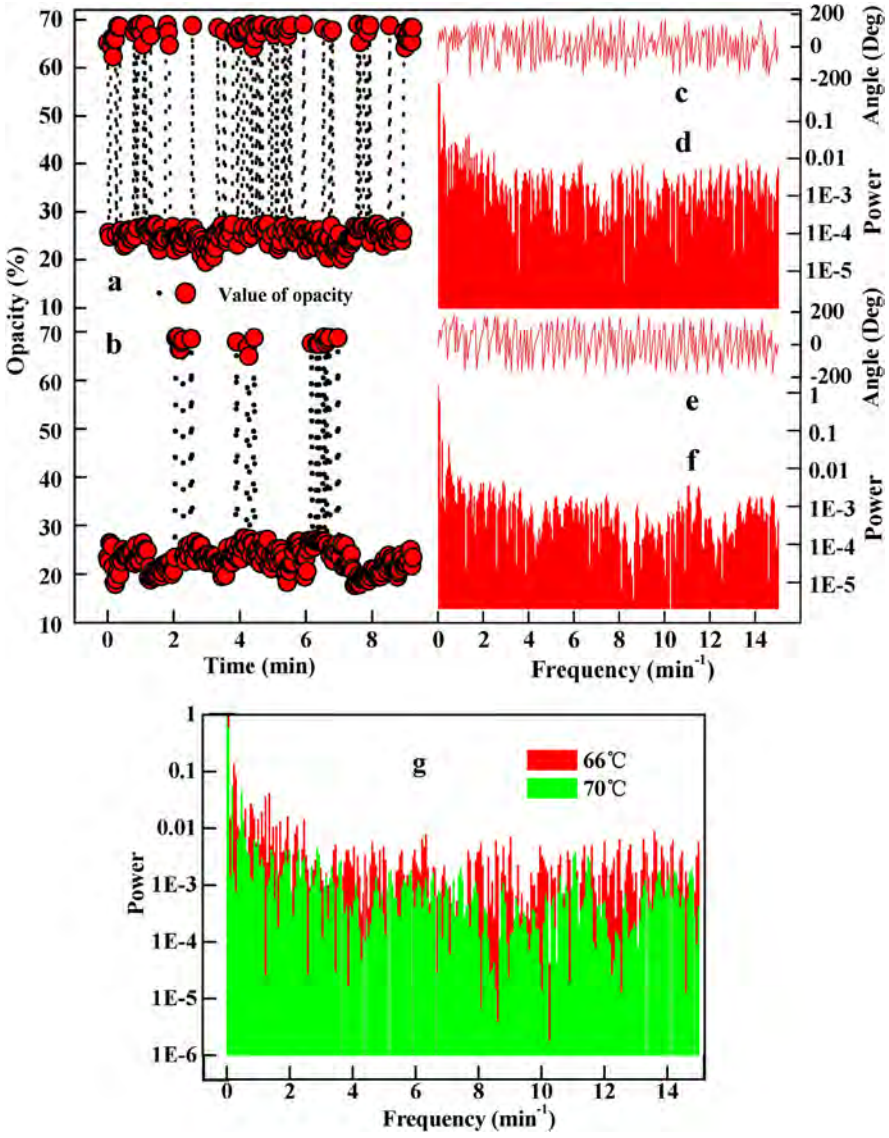

Fig. 4 – Diesel exhaust aerosols (DEA) opacity responses (a), (c), (d) at 66°C and (b), (e), (f) at 70°C. The time interval for collecting data is 2 sec. (a) and (b) belong to the time-domain information of the DEA opacity responses; (c), (d), (e), (f) and (g) belong to the frequency-domain information of the DEA opacity responses.

2.2. *Experimental original time series opacity data and the aggregated particles*

As the practical representation of the time-series opacity data on the complex system, the temperature effects on the aggregation process at the other four CTs are represented by the original experimental opacity data in Fig. 5, shown respectively from a to d. Fig. 5 shows the DEA opacity responses in the time-domain at the other four CTs 58, 64, 68 and 72°C. Combined with the opacity responses at 66 and 70°C, the six different CTs represent the CT range from 58 to 72°C, and respectively correspond to six different temperature effects.

Similar to the two characteristic values shown in Fig. 4a and b, the opacity values at the six CTs are generally divided into two sets, those larger than 60% and those less than 30%. Depending on the obviously dissimilar opacity variations with time at the six CTs, the DEA aggregation processes due to temperature effects are different under different temperature conditions. Different opacity variations correspond to different concentration variation for DEA aggregation, which indicates the result of the action of different effects on the DEA aggregation process.

In the measured data, it can be seen that the two sets of opacity data essentially reach two values of 30% and 60%. This behavior might result from aerosol trapping and aggregation growth at the nodal points of the ASW. With the size increase of particles in the aggregation process, the trapping action based on the acoustic radiation force Eq. (1) is gradually attenuated with the increase of Stokes drag force acting on particles. According to the drag force $F^s = 6\pi\mu a u_0$ (μ is the viscosity coefficient of the fluid; u_0 is the velocity of diesel

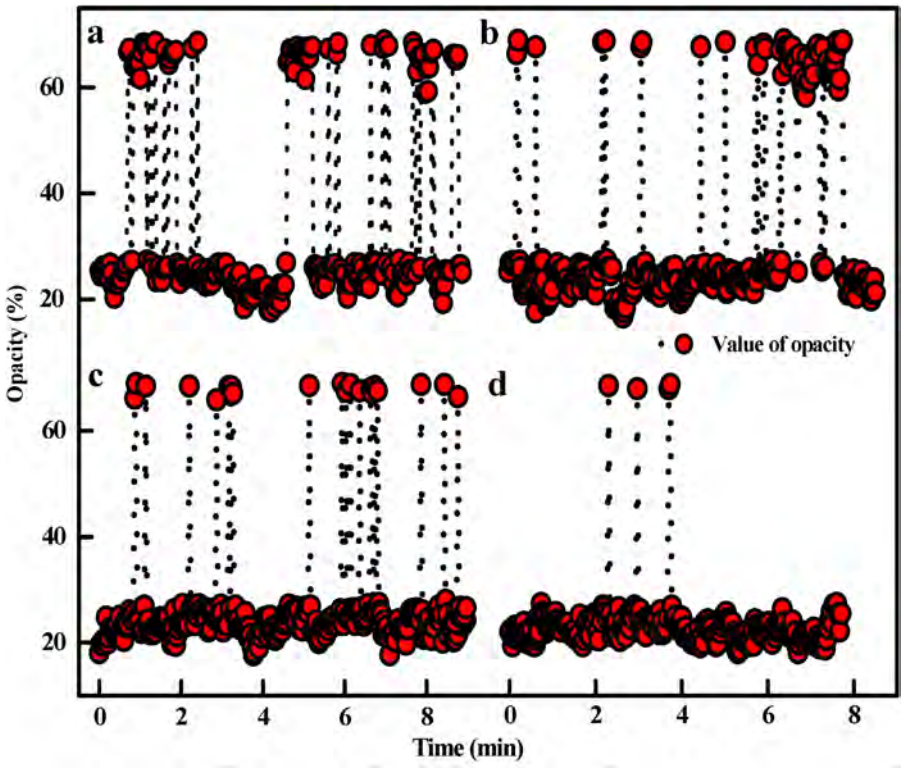

Fig. 5 – Time-domain information. (a) 58°C, (b) 64°C, (c) 68°C and (d) 72°C.

exhaust in CAC), the aggregated particle would move along the flow direction of the diesel exhaust when the grown particle becomes large enough and suddenly breaks away from the trapping action. Due to the concentration increase at the nodal point in the process of the aerosol trapping and aggregation growth, the sudden change before and after movement can cause two different concentration values for the opacity.

In terms of the aggregated particles, a typical particle size measurement at the CT of 66°C is shown in Fig. 6. The sample method depends on the stickiness of the film on the aggregated particles. As shown by this example, the particle sizes in Fig. 6a show that the sizes of the aggregated particles are about 2.491–68.17 μm. The aggregated particle size such as 68.17 μm is much larger than the well-known original DEA size distribution in the sub-micron range (Kittelson, 1998; Harris and Maricq, 2001; Wang et al., 2012). With higher magnification of a large particle of 68.17 μm, Fig. 6b shows that the aggregated particle is composed of small aggregates with sizes about 500.3–8833 nm. Fig. 6c shows that the small aggregates are composed of a large number of much smaller particles with sizes about 13.34–62.15 nm. The sizes of these nanoparticles are almost all in the original size range < 50 nm for the most of the DEA particle number (Guan et al., 2015; Burtscher, 2005; Kittelson, 1998; Harris and Maricq, 2001; Wang et al., 2012). The arrangement of these nanoparticles seems to be regular, as shown in Fig. 6d.

2.3. *Temperature tuning effect*

On the basis of Eq. (7), the probability distribution function for the opacity time-series data can be calculated using the time-domain information in the CT range from 58 to 72°C. The calculation result is shown in Fig. 7.

Fig. 7 shows the accumulation frequency distributions at the six CTs. For the time-series opacity data collected at 66°C, the accumulation frequency values (see Fig. 7a) rise rapidly to ~70%, but the increase of opacity is less than ~30% in the horizontal coordinate. The values remain constant at 70% until the opacity increases to 60%, and rise again to 100% as the opacity increases to greater than 60%. Such rise processes coincide with division of the opacity data into two opacity ranges of less than 30% and greater than 60% as analyzed in Section 2.2. According to the similar rise regulation at the other five CTs, it is easy to find that there are two discrete rise periods for the accumulation frequency distributions. Between the two rise periods, the accumulation frequency is approximately constant, which results in two data chains of low (opacity close to 30%) and high opacity value (opacity close to 60%) as shown in Fig. 7b. In the constant period, the value of the accumulation frequency at each CT weights the number of the opacity data respectively in the two data chains. This means that if the number of the opacity data is small at low opacity value, the number of the opacity data is large at high opacity value. A large number of opacity data at high opacity value indicates that the DEA concentration at the specific CT is large, and that the corresponding DEA aggregation process is violent. In the case of constant period, the value of the accumulation frequency at each CT can be used to quantify the aggregation level at the specific CT.

According to the quantification method at constant period, Fig. 8 shows the accumulation frequency variation at the six

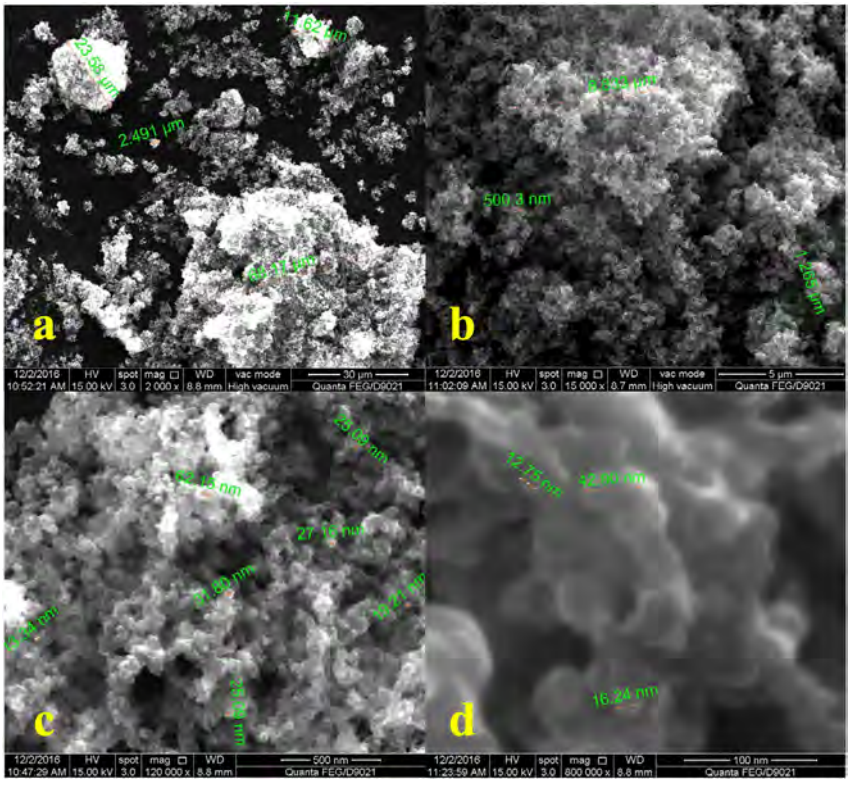

Fig. 6 – SEM (scanning electron microscope) images of the aggregated particles. (a), (b), (c) and (d) refer to different magnifications.

CTs. It can be seen that the DEA aggregation levels are sensitive to the CT, especially at the CTs of 66 and 68°C. The CT of 66°C corresponds to the smallest value of accumulation frequency, which means that the corresponding aggregation level is the most violent. The optimal aggregation in the CT range of 58–72°C is different from the monotonically increasing aggregation rate with temperature rise introduced in the aggregation model in the literature (Noorpoor et al., 2012). Combined with the maximum acoustic pressure at the CT of 66°C and the aggregation mechanism described in Section 1.2.1, the sub-resonance at 58 and 64°C, and the super-resonance at 68, 70 and 72°C might result in reduction of the aggregation level. According to Eqs. (1)–(4), the reason for the maximum agglomeration rate at 66°C may attribute to the maximum amplitude of acoustic pressure caused by the temperature tuning. In other studies, the effect of temperature on acoustic agglomeration is rarely noticed to be derived from the enhancement of agglomeration efficiency due to high acoustic pressure. For other acoustic devices acting as tube resonators possibly having a different L and n, when f_r = 1.286 kHz for Eq. (5), the maximum acoustic pressure and the optimum aggregation may be achieved at a different temperature T. Nevertheless, the process of using temperature tuning for acquiring the maximum acoustic aggregation rate is still universal. As an example, for a specific acoustic apparatus, the error of geometric parameters and the change of complex environment conditions with temperature would impact the resonance characteristic of the operating apparatus. The potential reduction of acoustic aggregation level caused by the geometric error and environmental change can be optimized by temperature tuning.

3. Conclusions

An acoustic apparatus integrated with a temperature tuning platform was constructed. The effect of temperature on the DEA aggregation process in an ASW field was studied using this apparatus. CTs in the range of 58–72°C were used to induce different aerosol aggregation processes with other parameters (such as the acoustic frequency of 1.286 kHz, voltage amplitude of 17 V and input electric power of 16.7 W) held constant. The temperature tuning focused on the CTs of 58, 64, 66, 68, 70 and 72°C. It was found that the DEA aggregation levels at the different CTs were different. The DEA aggregation process was found to be quite sensitive to the CT, and the optimal level of DEA aggregation could be achieved at 66°C. The size of the aggregated particles was much larger than the well-known submicron size of DEA. The optimal temperature effect for DEA aggregation in an ASW field attributes to the resonance occurring at 66°C. The enhancement effect of temperature tuning on aerosol acoustic aggregation processes can be used for other acoustic tube devices.

The aggregation result was shown by means of SEM (scanning electron microscope, Quanta 200 F, FEI, USA) imaging of the aggregated particles. The relationship of the aerosol aggregation process and opacity measurements was

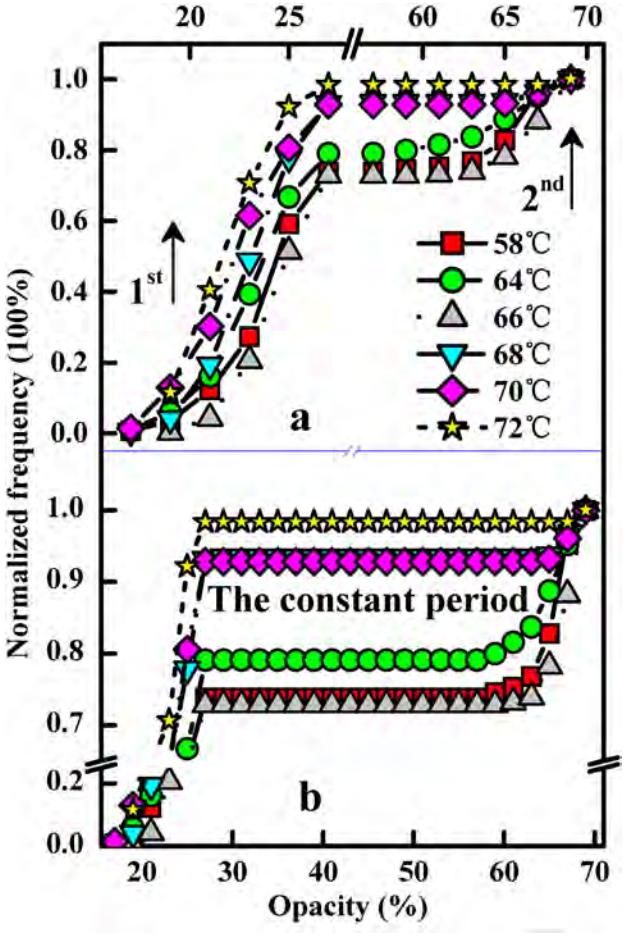

Fig. 7 – (a) Two rise periods, including the 1st rise period and the 2nd rise period, and (b) the constant period of the accumulation frequency distribution. For each CT, the total time for collecting data is at least 8 min; the value interval of statistical opacity is 2%; the total number of the data is larger than 250.

studied. The time-series opacity data of DEA at six CTs was used to characterize the variation regulation of DEA aggregation. The time-domain method and the frequency-domain

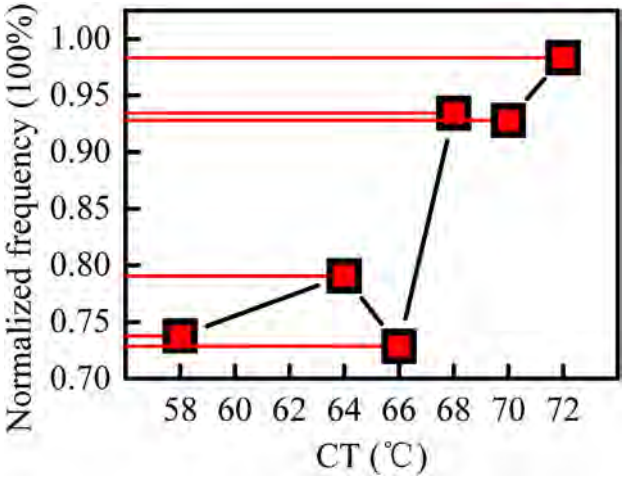

Fig. 8 – Accumulation frequency variation with CT.

method were used to analyze the opacity data acquired experimentally. The accumulation frequency distribution for the acquired time-series opacity data was used to further analyze the specific temperature effect. It is clear that the method and technology of aerosol acoustic aggregation process regulation and optimization through control of the operating temperature is feasible and convenient. On the other hand, the potential advantages of this technology not only could overcome the influence of errors from equipment manufacture and assembly, but also reduce the impact of complex running environments and seasonal changes on aggregation performance. The technique could be of value in industrial applications.

Acknowledgments

This work was supported by the National Nature Science Foundation of China (No. 11190015), the Scientific Research Foundation of Graduate School of Southeast University (No. YBJJ1547), the Research Innovation Program for College Graduates of Jiangsu Province (No. KYLX15_0069) and the Fundamental Research Funds for the Central Universities (Nos. 3203007706, 3203007206, 3203005101, 3203006701, 3203006711).

REFERENCES

Ahn, K.H., Ahn, J., Kim, I., Kang, S., Kim, S., Chu, K.H., et al., 2014. Separation of fine particles at different frequencies and HRTs using acoustic standing waves. Environ. Technol. 36, 302–309.

Beranek, L.L. (Ed.), 1954. Acoustics. McGraw-Hill Publishing Company.

Bruus, H., 2012. Acoustofluidics 7: the acoustic radiation force on small particles. Lab Chip 12, 1014–1021.

Burtscher, H., 2005. Physical characterization of particulate emissions from diesel engines: a review. J. Aerosol Sci. 36, 896–932.

Chen, H., Zhang, R., Cao, J., Shen, X., 2009. Experimental study on acoustic agglomeration of ultrafine particles in diesel engine exhaust. Neiranji Xuebao/Trans. CSICE (Chin. Soc. Intern. Combust. Engines) 27, 160–165.

Chen, H., Luo, Z., Jiang, J., Zhou, D., Lu, M., Fang, M., et al., 2015. Effects of simultaneous acoustic and electric fields on removal of fine particles emitted from coal combustion. Powder Technol. 281, 12–19.

Cheng, M., Dong, W., Qiao, Z., 2016. Experimental study on structured complex acoustic field and its effectiveness of particle manipulation. J. Southeast Univ. (Nat. Sci. Ed.) 46, 720–726.

Czechlowski, M., Golimowski, W., Sek, T., Szymanowicz, J., 2015. Exhaust opacity in a diesel engine powered with animal fats. Eksploat. Niezawodn. 17, 49–53.

Foresti, D., Sambatakakis, G., Bottan, S., Poulikakos, D., 2013. Morphing surfaces enable acoustophoretic contactless transport of ultrahigh-density matter in air. Sci. Rep. UK 3, 3176.

Gallego-Juarez, J.A., De Sarabia, E., Rodriguez-Corral, G., Hoffmann, T.L., Galvez-Moraleda, J.C., Rodriguez-Maroto, J.J., et al., 1999. Application of acoustic agglomeration to reduce fine particle emissions from coal combustion plants. Environ. Sci. Technol. 33, 3843–3849.

González, I., Gallego-Juárez, J.A., Riera, E., 2003. The influence of entrainment on acoustically induced interactions between aerosol particles—an experimental study. J. Aerosol Sci. 34, 1611–1631.

Gor'Kov, L., 1962. On the forces acting on a small particle in an acoustical field in an ideal fluid. Sov. Phys. Dokl. 6, 773–775.
Guan, B., Zhan, R., Lin, H., Huang, Z., 2015. Review of the state-of-the-art of exhaust particulate filter technology in internal combustion engines. J. Environ. Manag. 154, 225–258.
Guo, Q.J., Yang, Z.N., Zhang, J.S., 2012. Influence of a combined external field on the agglomeration of inhalable particles from a coal combustion plant. Powder Technol. 227, 67–73.
Hammarström, B., Laurell, T., Nilsson, J., 2012. Seed particle-enabled acoustic trapping of bacteria and nanoparticles in continuous flow systems. Lab Chip 12, 4296.
Harris, S.J., Maricq, M.M., 2001. Signature size distributions for diesel and gasoline engine exhaust particulate matter. J. Aerosol Sci. 32, 749–764.
Hawkes, J.J., Radel, S., 2013. Acoustofluidics 22: multi-wavelength resonators, applications and considerations. Lab Chip 13, 610–627.
Johansson, L., Evander, M., Lilliehorn, T., Almqvist, M., Nilsson, J., Laurell, T., et al., 2013. Temperature and trapping characterization of an acoustic trap with miniaturized integrated transducers – towards in-trap temperature regulation. Ultrasonics 53, 1020–1032.
Karpul, D., Tapson, J., Rapson, M., Jongens, A., Cohen, G., 2010. Limiting factors in acoustic separation of carbon particles in air. J. Acoust. Soc. Am. 127, 2153–2158.
Kittelson, D.B., 1998. Engines and nanoparticles: a review. J. Aerosol Sci. 29, 575–588.
Kozuka, T., Yasui, K., Tuziuti, T., Towata, A., Iida, Y., 2007. Noncontact acoustic manipulation in air. Jpn. J. Appl. Phys. 46, 4948–4950.
Kumar, M.S., Kerihuel, A., Bellettre, J., Tazerout, M., 2005. Experimental investigations on the use of preheated animal fat as fuel in a compression ignition engine. Renew. Energy 30, 1443–1456.
Laurell, T., Petersson, F., Nilsson, A., 2007. Chip integrated strategies for acoustic separation and manipulation of cells and particles. Chem. Soc. Rev. 36, 492–506.
Liu, J.Z., Zhang, G.X., Zhou, J.H., Wang, J., Zhao, W.D., Cen, K.F., 2009. Experimental study of acoustic agglomeration of coal-fired fly ash particles at low frequencies. Powder Technol. 193, 20–25.
Liu, J.Z., Wang, J., Zhang, G.X., Zhou, J.H., Cen, K.F., 2011. Frequency comparative study of coal-fired fly ash acoustic agglomeration. J. Environ. Sci. 23, 1845–1851.
Noorpoor, A.R., Sadighzadeh, A., Habibnejad, H., 2012. Experimental study on diesel exhaust particles agglomeration using acoustic waves. International Journal of Automotive Engineering 2, 252–260.
Qiao, Z., Huang, Y., Dong, W., 2014. Acoustic resonance characteristics of symmetric cylindrical waveguide with Helmholtz sound source. J. Southeast Univ. (Nat. Sci. Ed.) 44, 579–584.
Qiao, Z., Yaji, H., Vincenzo, N., Dong, W., 2015. Aerosol manipulation by acoustic tunable phase-control at resonant frequency. Powder Technol. 281, 76–82.
Sae, J., 1996. Recommended practice. Snap acceleration smoke test procedure for heavy-duty powered vehicles. Soc. Automot. Eng. 1996–2002.
Sheng, C.D., Shen, X.L., 2007. Simulation of acoustic agglomeration processes of poly-disperse solid particles. Aerosol Sci. Technol. 41, 1–13.
Sun, D.S., Zhang, X.D., Fang, L., 2013. Coupling effect of gas jet and acoustic wave on inhalable particle agglomeration. J. Aerosol Sci. 66, 12–23.
Wang, D., Liu, Z.C., Tian, J., Liu, J.W., Zhang, J.R., 2012. Investigation of particle emission characteristics from a diesel engine with a diesel particulate filter for alternative fuels. Int. J. Auto. Tech.-Kor. 13, 1023–1032.
Weiser, M., Apfel, R.E., Neppiras, E.A., 1984. Interparticle forces on red-cells in a standing wave field. Acustica 56, 114–119.
Yao, Q., Li, S.Q., Xu, H.W., Zhuo, J.K., Song, Q., 2010. Reprint of: studies on formation and control of combustion particulate matter in China: a review. Energy 35, 4480–4493.
Yuen, W.T., Fu, S.C., Kwan, J.K.C., Chao, C.Y.H., 2014. The use of nonlinear acoustics as an energy efficient technique for aerosol removal. Aerosol Sci. Technol. 48, 907–915.
Zajac, G., 2008. Influence of FAME addition to diesel fuel on exhaust fumes opacity of diesel engine. Int. Agrophys. 22, 179–183.